Cornell University Autonomous Underwater Vehicles: Design, Implementation, and Strategy of the Polaris and Sirius AUVs

Aaron Fink Adora Gao Akane Shirota Ana Hoffman Sole Andrés Blanco Angel Zhou Anthony Fei Anunth Ramaswami Aravind Ramaswami Braden Kennedy Coby Lai Collin Li Connor Lynaugh Danielle Xu Elizabeth Kelmenson Gabriel Mallare Grace Shirota Henry Wolf Ian Thomas Isabella Frank Jacqueline Wen Jeffrey Lederman Jeffrey Qian Joe Josh Faber Jueun Kwon Kammi Wong Karan Keerthy Karl Chen Katherine Knecht Kathryn Zhang Kavya Mittha Liza Kuntz Maggie Gao Matthew Hope Matthew Puzzini Michael Oji Miguel Roberts Nathaniel Navarro Nayoung Ha Parker Schless Ray Adam Sam Belliveau Sarah Grace Brown Sean Cavalieri Serena Zhang Sharon Wu Shawn Wang Shuyu Cao Vaishnavi Vednere Victoria Chan Victoria Stephens Wali Afridi Wei Ouyang Yvette Copeland

***Abstract*— Sirius and Polaris are the two autonomous vehicles representing Cornell University in the AUVSI RoboSub 2024 competition. Over the past year, CUAUV members have dedicated countless hours to building Sirius, our new 2024 AUV. Sirius' Upper Hull Pressure Vessel has been meticulously designed to increase accessibility and reduce room for error, sporting a new rectangular profile. We've designed and integrated a Battery Management System to prevent over current and minimize the risk of board damage. Additionally, our new servo-based actuation system promises greater reliability in completing missions. These advancements were made with the goal of making a system that is reliable and precise. An important strategic focus for this year is backwards compatibility in both the mechanical and electrical systems between the two vehicles. This supports the reliability of our systems as a whole.**

I. Competition Strategy

During last year's competition, many of our shortcomings were a result of our computer vision models lacking robustness to drastic changes in the lighting of the Transdec pool. Scattered light rays from the sun would change the brightness and tint of our camera feed, weakening the performance of our algorithms.

In this design cycle, a large focus was on improving our vision and actuation capabilities. Our newest vehicle, Sirius, was designed with the purpose of handling the more complex tasks that demand precise movement and actuation, including the bins, octagons, and torpedoes. On the other hand, we plan on offloading the simpler tasks, such as the buoy tasks and style points for gate to Polaris, our AUV from last year. Having already performed similar variants of these tasks in the past, this vehicle provides a high degree of reliability, allowing us to dedicate more time and energy on perfecting Sirius's missions.

As a large team with many dedicated engineers, CUAUV has the capacity to dedicate resources to many different projects simultaneously. We have a long-standing tradition of allowing all members, even new ones, to develop a component that will play a role on a competition AUV. For these reasons, along with the importance of both reliability and accuracy, having two AUVs makes the most sense. Our new system allows us to push the boundaries of complexity, testing out new components and strategies for completing competition tasks. And, simply by having two systems, we decrease the risk that any single electrical or mechanical failure cripples our ability to compete.

CUAUV is an ambitious team, and every year we approach competition with the desire to complete every task. Our subs are always fitted with the systems necessary to do so, and our software subteam develops the routines necessary to accomplish this goal. However, RoboSub is a difficult competition, and issues arise that make perfection impossible. Our focus as a team is to create redundancy to maximize our shot at using all of these systems and scoring as many points as possible.

II. Design Strategy

A. Mechanical Systems

The mechanical design of Sirius reflects a new approach to system design for our AUVs. A key aspect of this approach is reducing the overall number of enclosures and separate systems while preserving the AUV's modularity. Traditionally, our AUVs have been highly modular, with each subsystem isolated in its own enclosure. This design had advantages, such as preventing a single system's failure from compromising the entire AUV and ensuring backward compatibility. However, as seen with Polaris, which had separate enclosures for the zed camera, kill switch, gx sensor, and actuators, this approach led to difficulties in interfacing and maintenance, reliability issues, and unnecessary space consumption. By reducing enclosures, we can maintain modularity while improving reliability and efficiency.

Fig 1. Sirius Upper Hull Pressure Vessel.

Our Upper Hull Pressure Vessel (UHPV) exemplifies this new thinking. Instead of the traditional cylindrical UHPV, Sirius features a rectangular, lunchbox-style UHPV made by welding separate aluminum panels together. This design allowed us to integrate the kill switch, gx sensor, and ZED camera directly into the UHPV, significantly reducing the number of enclosures on the vehicle. Thus, the new UHPV is a major step toward our goal of reducing unnecessary enclosures. We also achieved our new system design goals through our approach to actuating the AUVs mechanisms. Instead of servo-driven hydraulics, we switched to directly driving our mechanisms with underwater servos, eliminating the need for a separate actuators' enclosure. Additionally, using a servo-driven camshaft to articulate spring-loaded restrainers, we integrated both torpedo firing and dropper release into a single mechanism. This approach has been crucial in achieving our new system design goals. The design is detailed in the Mechanical Appendix, as extensive math was done on the system to ensure its reliability.

Fig 2. Sirius torpedoes and droppers system.

Another core idea of our new system design is reducing the number of machined metal parts. While aluminum parts are strong, they take much longer to fabricate than 3D-printed parts. We have incorporated more 3D printing into our design where strength is not critical. For example, Sirius's racks inside the UHPV, previously made entirely of aluminum or sheet metal, now feature a central aluminum plate with 3D-printed components mounted onto it. This change drastically reduced the construction time for the racks, and also serves the purpose of cooling the UHPV. This is the first time we have added cooling into the racks, aiming to better protect the electrical boards while they're under constant use at competition.

Fig 3. Sirius racks, featuring 3D printed components.

Similarly, the torpedoes and droppers mechanism is now almost completely 3D-printed, except for components like the camshaft or restrainer shaft that experience considerable loads. This shift to 3D-printed components has allowed us to iterate

and test the mechanism more frequently, leading to a more refined and reliable system overall.

B. Electrical Systems

The electrical design choices behind both of our current AUVs emphasize customization and redundancy. Both feature modular layouts that enable "hot-swapping" of custom PCBs. This compartmental approach to electrical engineering enables CUAUV to rapidly integrate new features without a full redesign, making us responsive to the tasks of the competition. And, if a board fails, it can easily be replaced by a backup. The motherboards of our two competition AUVs are shown in figures 3 and 4.

Fig 4. 3D model of backplane on Sirius.

Fig 5. 3D model of updated backplane on Polaris.

1) Power System: CUAUV has taken a massive step forward in power management. Both of our AUVs load balance between two external battery pods, enabling continuous operation even if one dies. This year, each of our battery pods was fitted with a custom battery management system and OLED display. The BMS is built around the BQ40Z50 IC from TI, a chip that enables cell voltage balancing, battery health monitoring, reverse polarity protection, and much more. Internally, three newly designed rigorously tested hot-swappable PCBs handle power distribution. Last year, we encountered major issues due to underestimating power draw during operation and from an undesired short at competition. This year, the professional BMS system, major redesigns to the power path, and internal cooling fans will prevent these problems from arising again.

Fig 6. 3D model of BMB board located in battery pods.

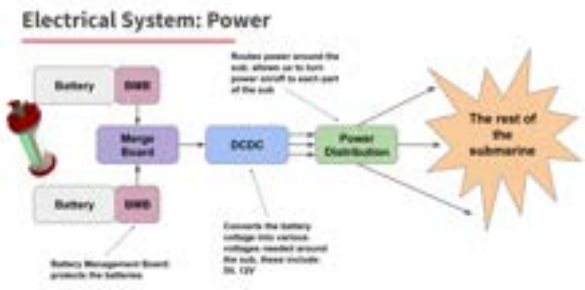

Fig 7. Layout of power system on Sirius and Polaris.

2) Additional Improvements: A wide array of redesigns and improvements from last year span the electrical systems of both AUVs. We improved the reliability of the actuator system, which is responsible for releasing torpedoes and markers, by using Blue Trail SER-2020 waterproof servo rather than hydraulics. To support this improvement, we redesigned the actuator PCB to output the required 7.4V 2.7A vs the 6V 830mA of the previous system. Additionally, the serial communication PCB of the AUV formerly output four USB channels, one for each onboard FTDI. This resulted in unnecessary cable clutter and required an external USB hub to integrate this data. Our new serial communication PCB integrates these channels internally using the TUSB4041I IC from TI, reducing the chances of user error and resulting in an overall more reliable system.

Fig 8. 3D model of updated actuator board.

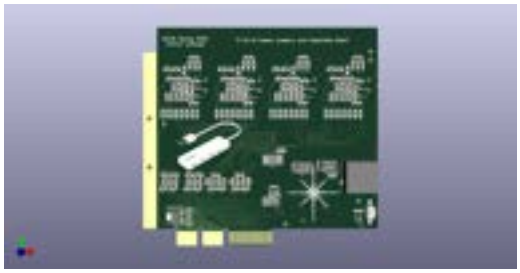

Fig 9. 3D model of updated serial board.

This year, the electrical team of CUAUV took a step back and examined the issues that have plagued our subsystems in the past, such as power management and unnecessary clutter. We thought creatively and came up with solutions that improve the reliability of our AUVs, make them easier to work with, and that integrate well with the ambitious goals of the rest of the team.

C. Software Systems

1) New Computer Vision Techniques: The integration of a new Jetson Orion NANO and stereo ZED camera on Sirius has enabled more powerful computer vision models in YOLO and depth sensing; with these new models, we have developed more robust methods of detecting mission elements [1]. For each mission element, we utilize YOLO to isolate where on the camera images the object of interest is located. Then, we utilize the ZED's depth sensing abilities to determine the precise location and orientation of the mission element relative to the AUV. With this positional information about the environment, the AUV can move to any desired orientation relative to the object, utilizing the DVL for accurate movement. This mission plan is a huge simplification from previous, complex strategies for positioning, where many sequences of centering and fine-tuning movements required more time and were more prone to error [2].

Fig 10. Diagram of our vision and mission systems.

2) Advanced color filtering: Furthermore, we have developed new color filtering techniques. First, we have integrated an auto-calibrate script that dynamically adjusts the exposure of the camera, which can mitigate changes in lighting from the sun. A white balance script, utilizing high pass filters on RGB color channels, can filter out warm hues that may be a result of the sun's location in the morning or evening. These two factors caused difficulty in last year's competition, and with these new additions, we became better prepared to adapt to the uncertain environmental conditions that the competition may bring.

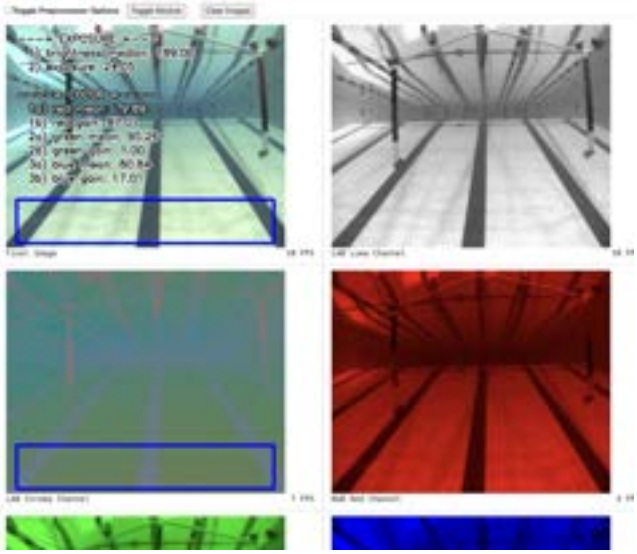

Fig 11. Various filters applied to camera output.

III. Testing Strategy

A. Electrical

This year, with the goal of improving reliability, we asked our senior electrical subteam members, each of whom worked on one of the historically

more challenging PCBs, to undergo a two-stage design process. Initial designs were populated and tested on the bench by March 10th, revealing a handful of issues. Of particular interest were PCBs featuring heavy redesigns, such as those on the power path. Both the battery management board and the merge board, which is responsible for load balancing, underwent thorough load testing, with the parameter for success being passing 60A for 10s and 30A continuously without major overheating (these values were based on current measurements from past AUVs). These boards did not meet the parameters for success and were majorly improved in the second design and testing stage, which lasted until April 20th. Both these and other PCBs passed testing procedures in the second testing stage, largely as a result of improvements made after the first.

Additionally, bench testing for all boards that communicate with the Jetson computer is made easy via the Serial Debugger. This is a piece of software written by CUAUV that communicates directly with the ATXMEGA MCU present on all of the "smart" PCBs. The program is able to read and write serial variables over RS232, providing accessible low-level control to our electrical team.

Finally, the aforementioned modular electrical design philosophy enables easy, reliable PCB testing. Throughout the year, the software team tests code in the pool using last year's AUV Polaris. Many of the new PCBs were compatible with this design and could be swapped in as they came online. This enabled the team to validate many of our designs in real-life conditions before the completion of our new competition AUV, with the thruster, actuator, led, and merge boards all tested before the end of the school year.

B. Mechanical

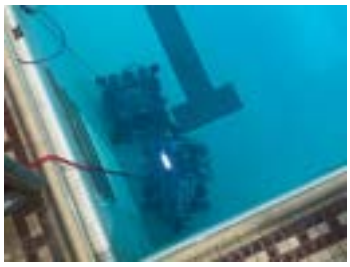

Fig 12. Leak test of the UHPVs.

Our mechanical testing primarily focuses on leak testing. Every enclosure with an O-ring seal must pass an overnight leak test before electrical integration. During the test, we line the inside of each enclosure with paper towels to easily identify any leaks by observing damp spots. Each enclosure is submerged and tested at 12 feet for 8 hours. After this period, we remove the enclosure from the pool, open the lid, and inspect the interior. If no water is detected inside, the project moves to the electrical integration phase. If water is found, we re-evaluate the seals and tolerances until the leak is resolved [3].

Our new lunchbox UHPV features over 20 O-ring seals. Due to limited overnight pool slots this year, the mechanical subteam devised a land-based leak testing method. By placing pressure gauges inside the UHPV, drawing a vacuum, and monitoring pressure changes, we efficiently identified problematic seals without the need for pool testing. Other leak testing methods include using soapy water to watch for bubbles and listening for hissing sounds while the vacuum is running. These multiple methods expedited the leak-free certification of the UHPV, allowing us to complete the testing within two weeks and proceed to electrical integration.

In addition to leak testing, we run simulations in SolidWorks on all our parts either with the pressure at 50 feet underwater or expected strain and collision forces to ensure all systems have an adequate safety factor. For example, the frame top plate has a FOS of 32 when 35 lbs are applied. The FOS of systems such as torpedoes and droppers are determined using torque and distance calculations, as highlighted in the Mechanical Appendix.

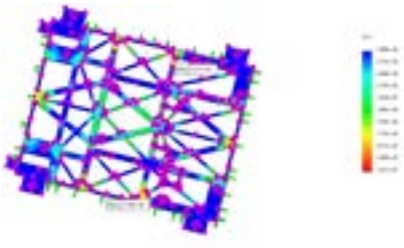

Fig 13. Frame top plate factor of safety.

Extensive testing and adaptation are also performed on our mechanisms. We collaborate closely with the electrical and software teams to ensure

servos and software are properly calibrated with the mechanisms. This year, our torpedoes and dropper cam systems underwent multiple revisions and rounds of collaborative testing to ensure system reliability. Reference the Mechanical Appendix for further details.

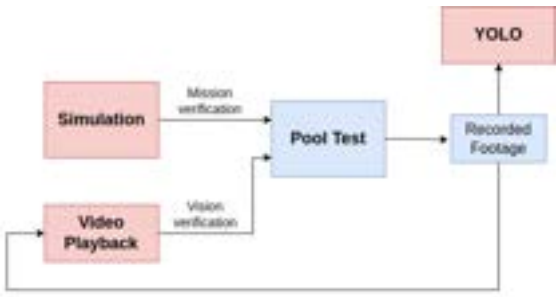

Fig 14. Software testing loop.

C. Software

When developing our mission logic, we utilize a 3D simulator that we have developed from scratch many years ago. We can simulate our missions on our own computers to verify the correctness of the core components.

When the fundamental logic is in place, we further test our missions in the pool to fine-tune our vision algorithms [4] and consider any edge cases the simulations may not have accounted for, since the simulator is a rather ideal environment. Testing our competition strategy is done bottom-up. We begin by running each individual task, from the gate, buoy, torpedoes, etc. on their own, assuming that the mission elements are in sight and verifying the submarine completes each task successfully given this precondition. When all tasks have been thoroughly tested, we chain the tasks together in one "master" mission, handling edge cases and searching logic.

While actively running our missions, we simultaneously record the camera footage in the background, which serves two purposes. First, we splice the videos into many frames and obtain more tagging data for our YOLO models. Second, using this footage, we can test our vision code on our local systems as well, using a video playback application that we have developed. Since pool time is limited, this application allows us to test our vision models without constraint. This creates a testing loop: after each pool test, we revisit the simulator and video player to made adjustments while not in the pool, better preparing our code for the next pool test and continuously improving until we are ready for competition.

IV. Acknowledgements

CUAUV would like to thank all the individuals and organizations who have supported us over the past year, including Cornell's MAE, ECE, and CS departments. Thank you to the Fischell family for their ongoing support and for sparking a lifelong interest in AUVs in our team members. CUAUV would especially like to thank our adviser: Professor Hunter Adams. Special thanks to the Director of Cornell Aquatics, Brigitta Putnam; the MAE Director of Instructional Laboratories, Matt Ulinski; Cornell Engineering's administrative staff, especially Kae-Lynn Buchanan Wilson and Karen Prosser, and last but not least, the Cornell Rapid Prototyping Lab (RPL). For their tremendous support in the absence of a Swanson Project Team Director, we would like to give special thanks to Lauren Stulgis, Kate Reiter, and Gibran el-Sulayman. We would also like to thank all of our corporate sponsors, without whom we would not be able to compete. Platinum Sponsors: Cornell University; Portwell. Gold Sponsors: iFixit. Silver: Polymer Plastics Company, LC. Bronze: BlueRobotics, Varda Space Industries, Savox, Datron, and Acbotics Research.

References

[1] D. Reis, J. Kupec, and J. Hong, "Real-time flying object detection with YOLOv8," arXiv preprint arXiv:2305.09972, 2023.
[2] A. Wang et al., "Yolov10: Real-time end-to-end object detection," arXiv preprint arXiv:2405.14458, 2024.
[3] Parker O-Ring Handbook, ORD 5700. Parker Hannifin Corporation, Lexington, KY, USA, 2021
[4] G. Bradski and A. Kaehler, OpenCV. Dr. Dobb's journal of software tools, vol. 3, no. 2, 2000.
[5] B. Benson, "Design of a Low-cost Underwater Acoustic Modem for Short-Range Sensor Networks," 2010.

APPENDIX A

Component	Vendor	Model/Type	Specs	Source	Cost	Year
Frame	Datron	Custom Aluminum Waterjet	Custom	Custom	Sponsored	2024
Aluminum Stock	Midwest Steel	Various	Various	Purchased	$850	2024
Aluminum Anodization	Surface Finish Technologies	N/A	N/A	Purchased	$1,675	2024
Acrylic Tubing	Polymer Plastics	N/A	Custom	Custom	Sponsored	2024
Waterproof Connectors	SEACON HUMMER/ WET-CON	Dry/Wet connectors	Custom	Custom	$1,675	2018
Thrusters + Propellers	Blue Robotics	T200	Brushless Thruster	Purchased	$2,312	2018
Motor Control	Blue Robotics	Basic ESC	Speed Control	Purchased	$400	2018
Actuators	Blue Trail	SER-2020	230º Underwater Servo	Purchased	$495	2024
Battery	HobbyKing	Multistar 4S	High Capacity, LiPo Battery	Purchased	$165.90	2018
Battery Management Chip	TI	BQ40Z50	Battery Management	Purchased	$7	2024
DC Voltage Regulator	Cincon	CHB75-12S12	Voltage Regulation	Purchased	$76.28	2024
CPU/GPU	NVIDIA	NVIDIA Jetson TX2	Six 2GHz, Arm8Cores	Purchased	Sponsored	2018
CPU/GPU	NVIDIA	Jetson Orin Nano	Six 2GHz, Arm8Cores	Purchased	$500	2023
Compass and IMU	LORD Microstrain	3DM-GX3 / 3DM-GX5	AHRS	Purchased	Sponsored	2018

Component	Vendor	Model/Type	Specs	Source	Cost	Year
Cameras	IDS	UI-6230SE UI-5140CP,	Cameras	Purchased	Sponsored	2018
Camera	FLIR	BFS-PGE-16S2C-CS Blackfly S GigE	Cameras	Purchased	$175	2024
ZED Camera	StereoLabs	Zed 2i	Cameras	Purchased	$499.99	2024
Hydrophones Processor	NXP	FRDM-K64F	Hydrophones	Purchased	$52.35	2024
Hydrophones, Teledyne Marine	RESON	Acoustic transducers	Hydrophones	Purchased	N/A	2018
High Level Control	CUAUV	6-DOF Dual Quaternion and YPR	Linear Least Square PID	Custom	N/A	2015
Vision Algorithm	OpenCV	OpenCV4	Transparent GPU Support	Purchased	Free	2024
Vision Algorithm	YOLO	YOLOv8	Transparent GPU Support	Purchased	Free	2024
Depth Sensing	ZED	ZED SDK 4.1	N/A	Purchased	Free	2024
Acoustics	CUAUV	Custom DSP	N/A	Custom	Free	2024
Localization and Mapping	Mur-Artal	ORB-SLAM2	Modified	Purchased	Free	2024
Autonomy	CUAUV	Mission Planning system	N/A	Custom	Free	2024
Software	CUAUV/FSF	GNU	N/A	Custom	Free	2024

Appendix B: Mechanical Appendices

A Purpose

The Mechanical Appendices showcase the new projects and improvements that were made to our systems this year. Switching to underwater servo actuation and a lunchbox style UHPV required major redesigns of all systems. The following pages further detail design choices and testing, highlighting our major mechanical progress this year.

B Sirius Torpedoes and Droppers

Figure 1: Sirius Torpedoes and Droppers

The Sirius torpedoes and droppers mechanism gives our submarine the ability to complete two tasks at competition. First, our sub must fire a pair of torpedoes through cardboard cutouts. Second, our sub must release a pair of droppers into a bin located at the bottom of the competition pool. Traditionally, our submarine has two distinct mechanisms to accomplish each task. This year, our submarine utilizes a novel servo-actuated mechanism that performs both tasks. The mechanism works by employing a sequence of cams to actuate a series of restrainers that hold and release our sub's droppers and spring-powered torpedoes.

B.1 Actuation Sequence

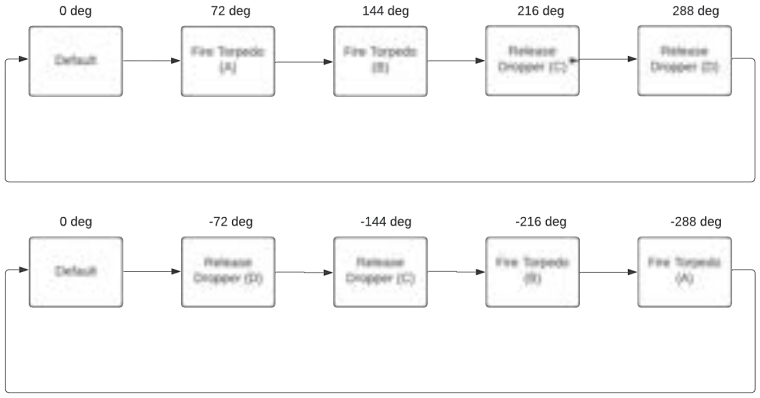

Figure 2: Torpedoes and Droppers State Diagram. The top sequence demonstrates launching the torpedoes first. The bottom sequence demonstrates launching the droppers first. The letters correspond to system states. The corresponding physical system states are shown below.

(a) Cams state default (b) Restrainers state default

Figure 3: The left image depicts the default state of the cams. The right image depicts the default state of the restrainers. In this state, the torsion springs are pushing on the restrainers holding both the torpedoes and droppers in place.

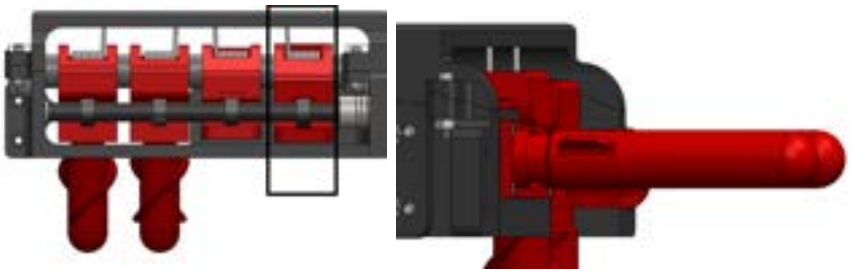

(a) Cams state A (b) Restrainers state A

Figure 4: The left image depicts the cam state for launching the first torpedo. The right image depicts the corresponding restrainer state.

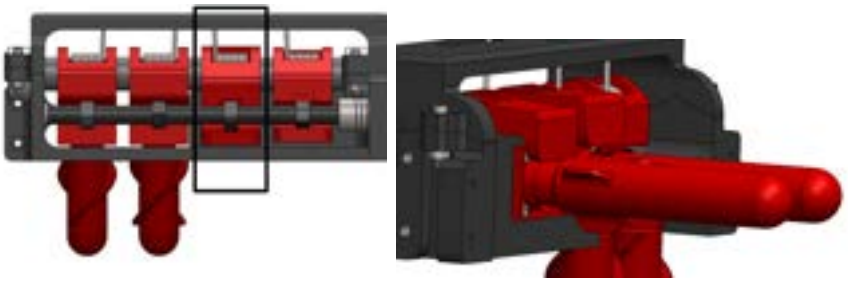

(a) Cams state B (b) Restrainers state B

Figure 5: The left image depicts the cam state for launching the second torpedo. The right image depicts the corresponding restrainer state.

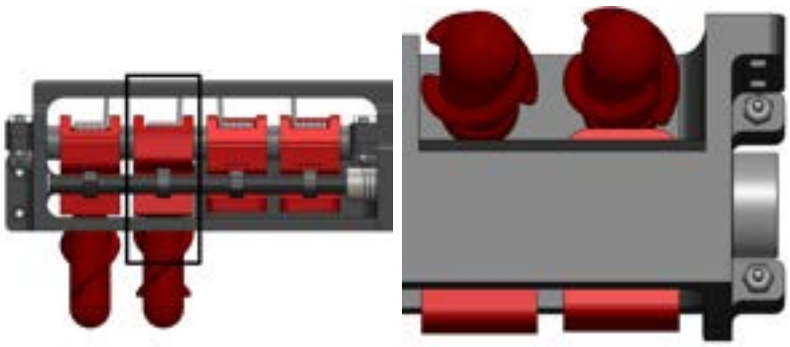

(a) Cams state C (b) Restrainers state C

Figure 6: The left image depicts the cam state for releasing the first dropper. The right image depicts the corresponding restrainer state.

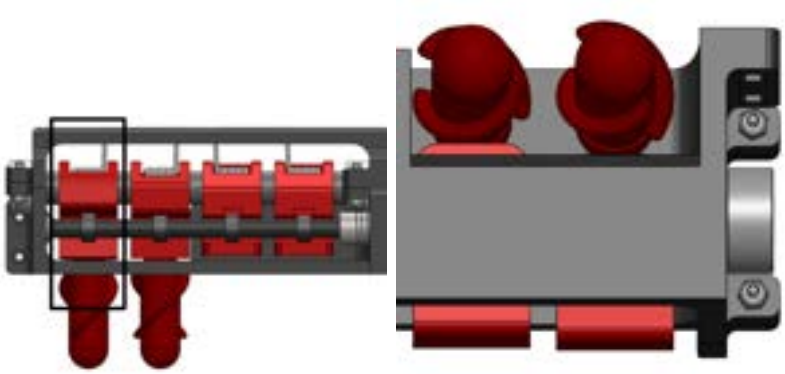

(a) Cams state D (b) Restrainers state D

Figure 7: The left image depicts the cam state for releasing the second dropper. The right image depicts the corresponding restrainer state.

B.2 Analysis

B.2.1 Theoretical Analysis

The purpose of the theoretical analysis shown in this section is to justify a set of requirements essential for the TD mechanism to function. The criteria are outlined below.

- The torsion springs must supply sufficient torque such that the torpedo restrainers can hold the torpedoes in place.
- The torsion springs must supply sufficient torque such that the dropper restrainers can hold the droppers in place,
- The servo must supply sufficient torque to raise the torpedo restrainers and launch the torpedoes.
- The servo must supply sufficient torque to raise the dropper restrainers and release the droppers. In order to perform the calculations, the following parameters were measured from the TD mechanism.

Table 1: Measured Parameters

Torpedo Lever Arm	t_{lever}	0.307 in
Dropper lever Arm	d_{lever}	0.307 in
Max Linear Spring Force	F_{st}	9.9 lb
Weight of Torpedo	w_t	0.05 lb
Weight of Dropper	w_d	0.07 lb
Angular Deflection of Torpedo Cam	θ_{ct}	44.97 deg
Angular Deflection of Torpedo Restrainer	θ_t	4.59 deg
Angular Deflection of Dropper Cam	θ_{cd}	38.69 deg
Angular Deflection of Dropper Restrainer	θ_d	5.22 deg
Friction in Camshaft	F_c	3 inlb
Max Servo Torque	τ_s	29 inlb
Torsion Spring Torque	τ_{sp}	5.24 inlb
Coefficient of Friction between ABS and Aluminum	μ_s	0.6
Radius of restrainer shaft	r	0.25 in
Weight of Dropper Restrainer	$w_d r$	0.12 lb
Weight of Torpedo Restrainer	$w_t r$	0.07 lb

From geometry and fundamental physics principles, we can derive the following relationships.

Table 2: Additional Equation Variables

Torque Torpedo Applies to Restrainer	τ_{torp}
Torque Dropper Applies to Restrainer	τ_{drop}
Frictional Torque in Restrainer Shaft	τ_{rs}
Safety Factor for holding a torpedo	γ_{ht}
Safety Factor for holding a dropper	γ_{hd}
Safety Factor for launching a torpedo	γ_{lt}
Safety Factor for releasing a dropper	γ_{rd}

$$\tau_{torp} = -F_{st} t_{lever} + \tau_{sp} \tag{1}$$

$$\tau_{drop} = -w_d d_{lever} + \tau_{sp} \tag{2}$$

$$\tau_{rs} = 2(F_{st} + w_d + w_d r + w_t r)\mu_s r \tag{3}$$

Using the following equations, we can derive safety factors for holding a torpedo in place, holding a dropper in place, launching a torpedo, and releasing a dropper.

$$\gamma_{ht} = \frac{tau_{torp} + \tau_{rs}}{F_{st} t_{lever}} \tag{4}$$

$$\gamma_{hd} = \frac{tau_{drop} + \tau_{rs}}{F_{st} d_{lever}} \tag{5}$$

$$\gamma_{lt} = \frac{\tau_s}{\tau_{rs} + \tau_{torp} + F_c} \frac{\theta_{ct}}{\theta_t} \tag{6}$$

$$\gamma_{rd} = \frac{\tau_s}{\tau_{rs} + \tau_{drop} + F_c} \frac{\theta_{cd}}{\theta_d} \tag{7}$$

Using equations 4-7 and the measured parameters, we can compute each safety factor. The results have been summarized in the table below.

Table 3: Safety Factors

γ_{ht}	2.72
γ_{hd}	385.66
γ_{lt}	34.44
γ_{rd}	19.07

The table above shows that the TD mechanism design satisfies all its requirements with considerable safety factors.

B.2.2 Finite Element Analysis

The FEA below focuses on the loads placed on the restrainers and camshaft as these are the components most likely to break. The FEA simulates the effects of holding the torpedoes and droppers in place on the restrainer and dropper assemblies. Loads simulating the forces that the torpedoes and droppers exert on their restrainers were applied to the Solidworks simulation models. The results of the simulation are summarized in the table below.

As illustrated by the table, the design has a factor of safety of 2.7 with the lowest factor of safety located at the tips of the torpedo restrainers. This is expected as the torpedo restrainers are under considerable load and are made of 3D-printed material. Nevertheless, a 2.7 safety factor along with very tiny deformations in the TD dropper mechanism indicates that the restrainer and camshaft assemblies should be able to handle loads placed on them.

Table 4: Restainer and Cam Assembly FEA Results

Max Stress	21.31 MPa
Factor of Safety	2.74
Max Deformation	0.1086 mm

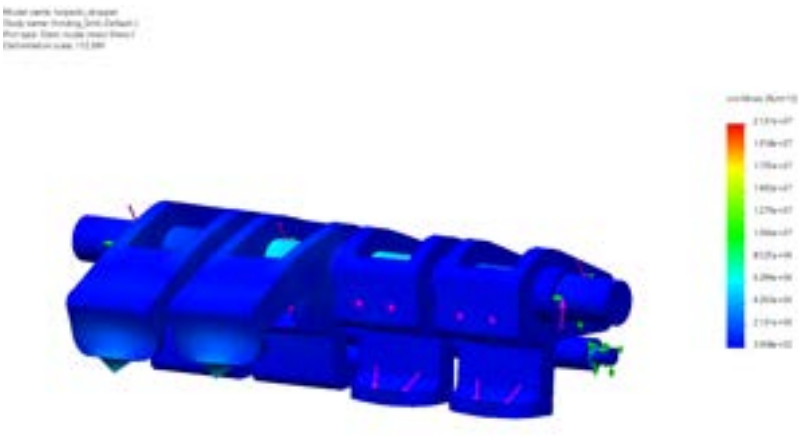

(a) Equivalent Von-Mises Stress

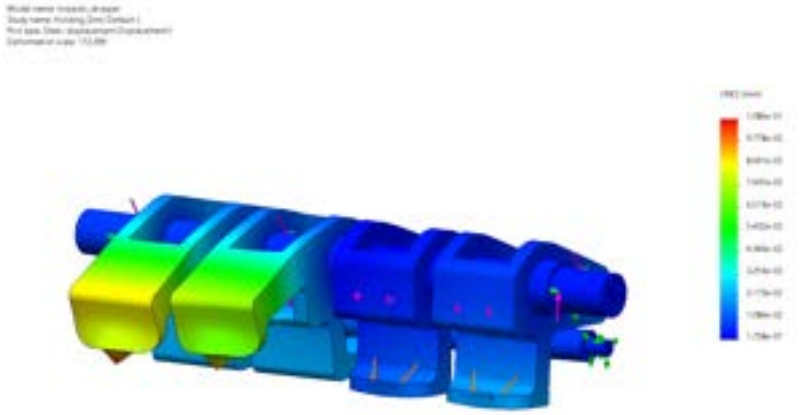

(b) Total Deformation

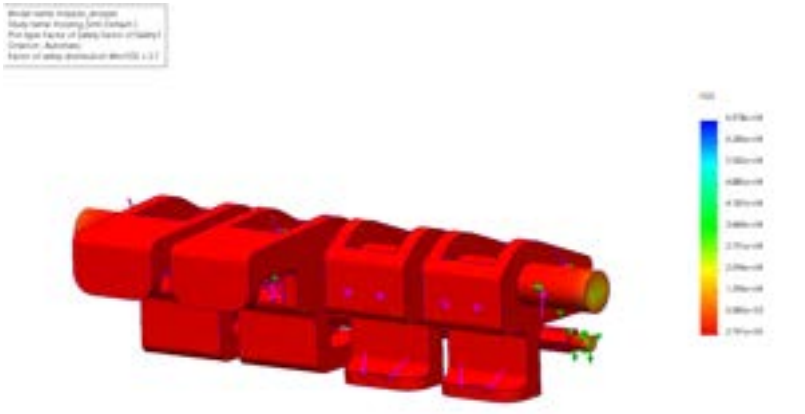

(c) Factor of Safety

Figure 8: Restrainer and Cam Assembly FEA Results

B.2.3 Fluid Flow Analysis

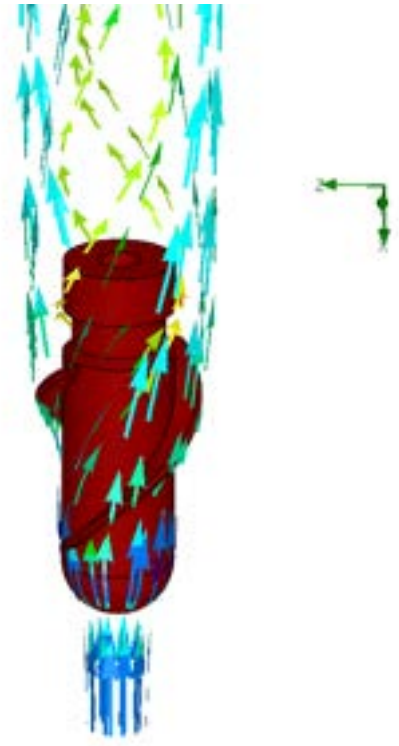

Figure 9: Streamlines of a 1 m/s fluid flow around the dropper.

The fluid flow analysis above depicts streamlines from fluid flowing at 1 m/s around a dropper. There is a clear helical streamline pattern around the fins of the dropper. Using Euler's equation for fluid flow in normal coordinates, we can show that bending streamlines exert torque on a hydrofoil.

$$\frac{\partial k}{\partial n} = -\frac{\rho U^2}{R} \tag{8}$$

This equation demonstrates that a fluid that bends in a circle has a Bernoulli constant k that decreases with smaller radii of curvature. Since there is not much change in gravitational potential energy along streamlines of different radii, the pressure along streamlines closer to the fins have lower pressure as they have smaller radii. This causes a torque to be exerted on the fins of the dropper causing the dropper to rotate. This rotation of the dropper along its axis will hopefully improve its stability.

B.2.4 Torpedo Range Analysis

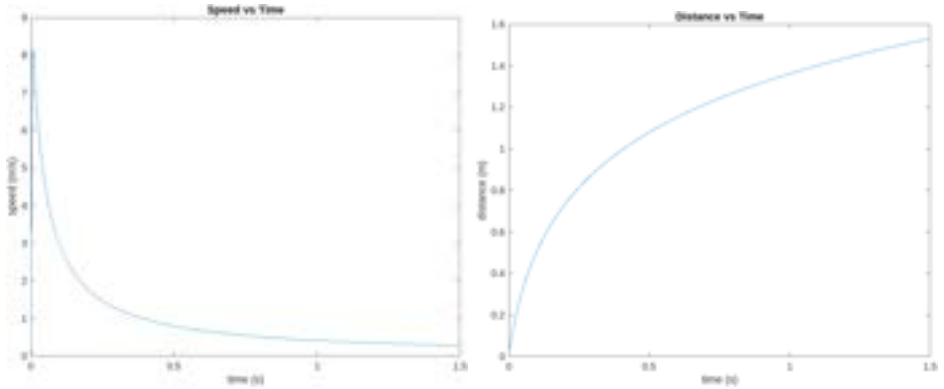

(a) Speed Plot (b) Distance Plot

Figure 10: Distance and speed that torpedo travels over 1.5 s

The dynamics of a torpedo launched by the mechanism are governed by the drag force and spring force on the torpedo. These forces can be used to construct the set of differential equations shown below.

Table 5: Equation Variables

m	Mass of torpedo
k	Spring constant
l	Relaxed length of spring
ρ	Density of water
C_d	Drag coefficient
A	Reference area

$$\begin{cases} m\ddot{x} = k(l-x) - \frac{1}{2}\rho\dot{x}^2 C_d A & x < l \\ m\ddot{x} = -\frac{1}{2}\rho\dot{x}^2 C_d A & x \geq l \end{cases}$$

Using ode45 to simulate the above set of differential equations in Matlab, we can obtain plots for the position and velocity of the torpedo as shown above. The torpedo's motion was simulated over 1.5 s because, at timescales longer than this, other hydrodynamic effects begin to significantly affect the accuracy of the torpedoes. As shown by the distance plot, the torpedo travels 1.5 m or 4.92 ft in 1.5 s. Typically, our submarine launches at its target from about 1ft. Therefore, the torpedo launch mechanism should be able to provide more than enough range and accuracy to the torpedoes in order to hit targets at 1 ft reliably.

C Polaris Torpedoes and Droppers

Figure 11: Polaris Torpedoes and Droppers

The Polaris Torpedo and Droppers Subsystem is responsible for completing two different tasks at the Robosub competition. The torpedo subsystem is responsible for firing two torpedoes through two cut out holes at the competition. The Dropper subsystem is responsible for dropping two droppers (essentially heavier and wider torpedoes) into specified bins. The overall system can fire the torpedoes (T) and droppers (D) into two specific orders. They can either be fired T - T - D - D (Torpedoes first, then Droppers) or D - D - T - T (Droppers first, then Torpedoes). The goal of the torpedo and droppers system is to securely hold both the droppers and torpedoes using only one underwater servo, and fire them on command when the submarine is completing the torpedo or dropper tasks.

C.1 Actuation Sequence

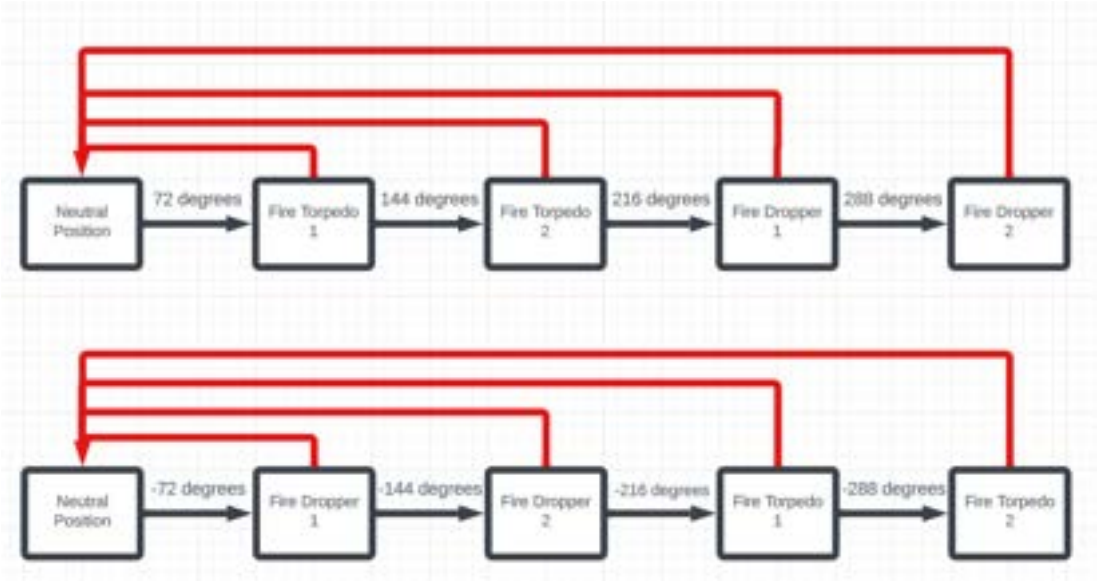

Figure 12: State Diagram for the full system. The angles represent what servo angle is necessary to reach the specified state. The red lines from each state tell how to return the system to its neutral position from each state.

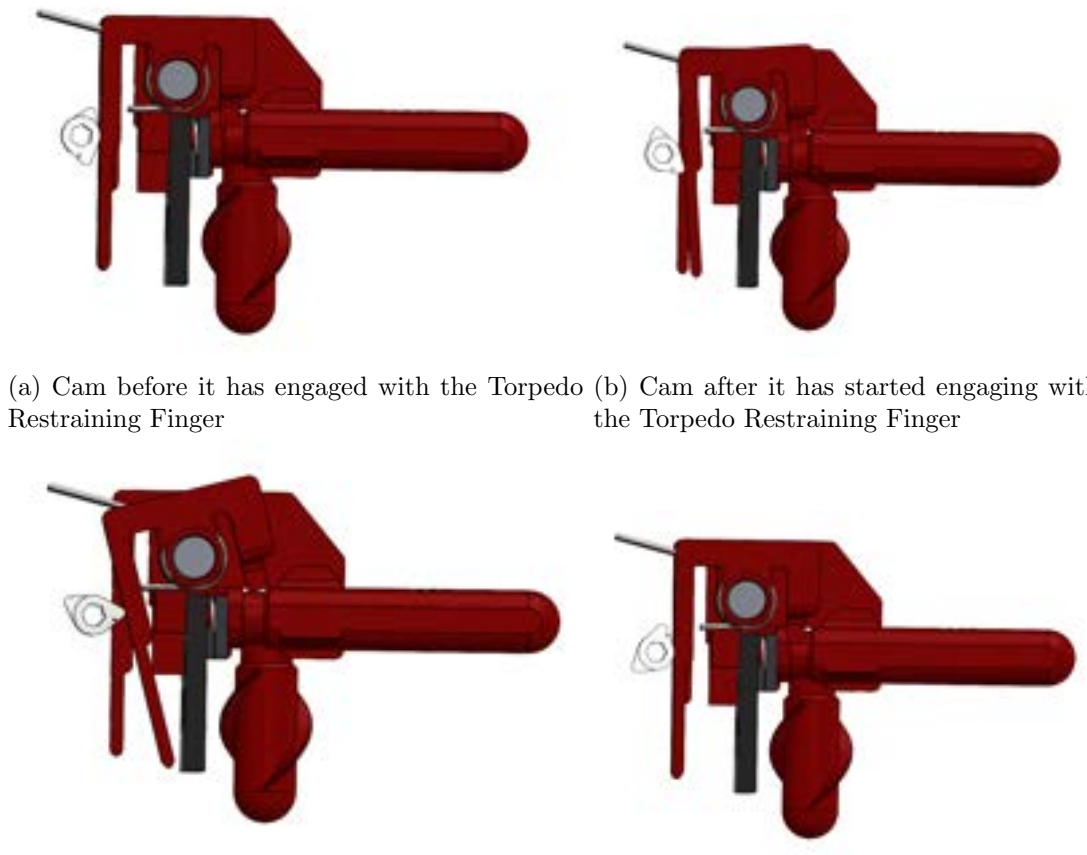

(a) Cam before it has engaged with the Torpedo Restraining Finger

(b) Cam after it has started engaging with the Torpedo Restraining Finger

(c) Cam after it has lifted the Torpedo Restraining Finger to its maximum deflection

(d) Cam after it has returned the Torpedo Restraining Finger to the original position

Figure 13: Shows the full procedure of a Cam lifting and lowering a Torpedo Restraining Finger

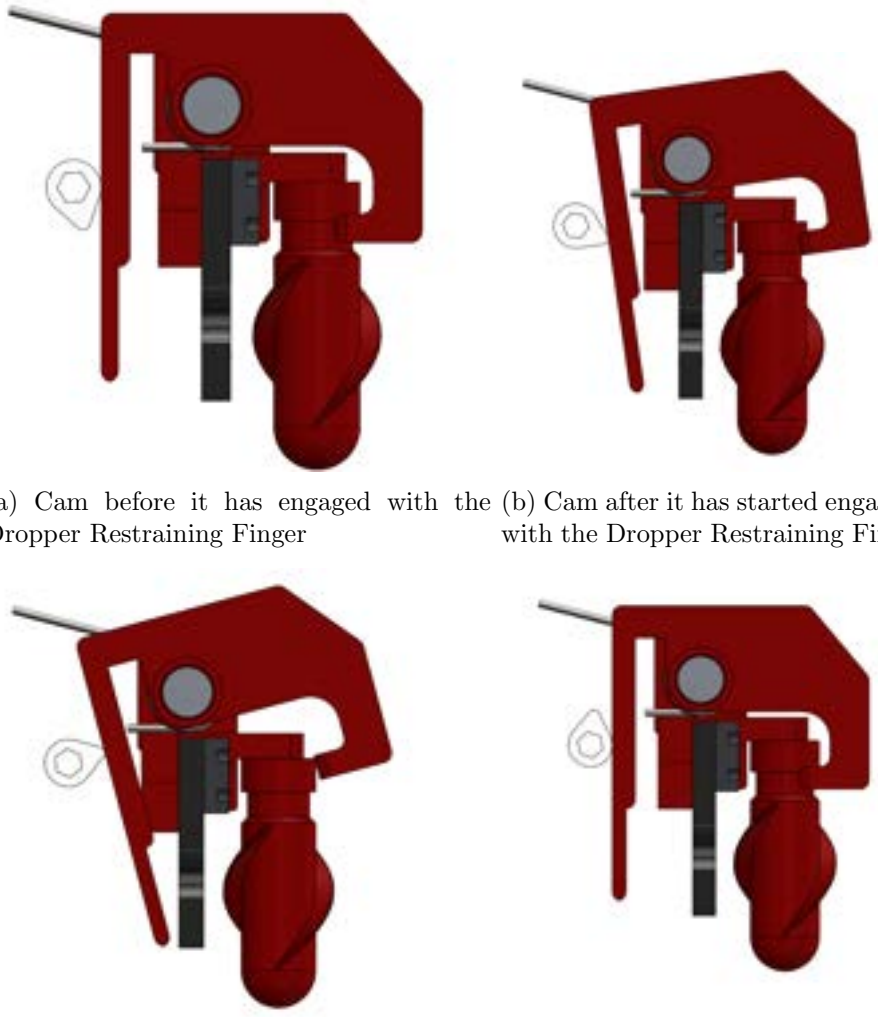

(a) Cam before it has engaged with the Dropper Restraining Finger

(b) Cam after it has started engaging with the Dropper Restraining Finger

(c) Cam after it has lifted the dropper restraining bar to its maximum deflection

(d) Cam after it has returned the Dropper Restraining Finger to the original position

Figure 14: Shows the full procedure of a Cam lifting and lowering a Dropper Restraining Finger

C.2 System Analysis

C.2.1 Torpedo/Dropper Holding & Release

A mathematical analysis was performed on the system to ensure it met design requirements. In particular, this system had to satisfy the following design requirements in order to fulfill its larger system level requirements specified in **??**.

- The torsion springs must provide enough torque to securely hold the torpedoes in place against the compression springs
- The torsion springs must provide enough torque to securely hold the droppers in place against their weight
- The servo must provide enough torque to lift the torpedo restraining bar to fire the torpedoes
- The servo must provide enough torque to lift the dropper restraining bar to release the droppers

To run this analysis, I have defined the following system parameters and safety factors that will be used in the analysis below. All units are in imperial for this table

‘ Symbol	Description	Value.
l_d	dropper lever arm	0.4
l_t	torpedo lever arm	0.9125
w_t	torpedo weight	0.044
w_d	dropper weight	0.05
$w_{restrainer,t}$	torpedo restraining finger weight	0.12
$w_{restrainer,d}$	dropper restraining finger weight	0.07
$\theta_{cam,t}$	torpedo cam angle change	72
$\theta_{cam,d}$	dropper cam angle change	72
$\theta_{restrainer,t}$	torpedo restraining finger angle change	14.05
$\theta_{restrainer,d}$	dropper restraining finger angle change	14.05
τ_{cam}	cam shaft friction torque	3
τ_{servo}	servo friction torque	29
τ_{spring}	torsional spring torque	8.9375
F_{spring}	compression spring force	9.9
r_{shaft}	radius of restraining finger shaft	0.25
$\mu_{ABS,Al}$	coefficient of friction between ABS and 6061 T6 Aluminum	0.6

‘ Symbol	Description.
$\eta_{torpedoholding}$	torpedo holding safety factor
$\eta_{dropperholding}$	dropper holding safety factor
$\eta_{torpedorelease}$	torpedo release safety factor
$\eta_{dropperrelease}$	dropper release safety factor

Analyzing the moment on the restraining bar shaft, we can solve for the safety factors of interest for the system. First, we can compute the net torque on the torpedoes and droppers. Next, we can compute the friction inside the restraining shaft assembly. With these values, we can find the four safety factors listed in the table above. The mechanical advantage of

the cams was approximated by taking the ratio of the angle change in the cams to the angle change in the restraining fingers.

$$\tau_{torpedo} = -F_{spring} * l_t + \tau_{spring} \tag{9}$$

$$\tau_{torpedo} = -w_d * l_d + \tau_{spring} \tag{10}$$

$$\tau_{restrainershaftfriction} = 2 * (F_{spring} + w_d + w_t + w_{restrainer,t} + w_{restrainer,d}) * \mu_{ABS,Al} * r_{shaft} \tag{11}$$

$$\eta_{torpedoholding} = \frac{\tau_{torpedo} + \tau_{restrainershaftfriction}}{F_{spring} * l_t} \tag{12}$$

$$\eta_{dropperholding} = \frac{\tau_{dropper} + \tau_{restrainershaftfriction}}{w_d * l_d} \tag{13}$$

$$\eta_{torpedorelease} = \frac{\tau_{servo}}{\tau_{restrainershaftfriction} + \tau_{torpedo} + \tau_{cam}} * \frac{\theta_{cam,t}}{\theta_{restrainer,t}} \tag{14}$$

$$\eta_{dropperrelease} = \frac{\tau_{servo}}{\tau_{restrainershaftfriction} + \tau_{dropper} + \tau_{cam}} * \frac{\theta_{cam,d}}{\theta_{restrainer,d}} \tag{15}$$

With the lengths shown in the table above, we can compute the safety factors for this design with a large safety factor for each requirement.

‘ Symbol	Description.
$\eta_{torpedoholding}$	3.0284
$\eta_{dropperholding}$	261.853
$\eta_{torpedorelease}$	13.052
$\eta_{dropperrelease}$	9.634

From the table above, we can see that this design will meet the necessary design requirements.

C.2.2 Torpedo Distance Analysis

I performed an analysis on the range of the torpedoes to determine their range to ensure that they met operational parameters. To determine the range, I used a force balance to derive the differential equations governing the dynamics of the system. After deriving the differential equations, I used ode45 in MATLAB to simulate the position and velocity of the torpedoes over time and generate the plots shown in Figure 1. The following table shows the constants and their values that are used when deriving the dynamics of the system. The drag coefficient was approximated as the drag coefficient for a sphere since the front of the torpedo is a hemisphere. All units are in imperial.

‘ Symbol	Description	Value.
k	spring constant	6.58
l	uncompressed length of the spring	2.75
m	torpedo mass	0.044
A	cross sectional area of the torpedo	0.4417
ρ	density of water	62.4
C_d	drag coefficient	0.45

To derive the dynamics, there are two different domains. While the position of the torpedo is less than the natural length of the spring, the torpedo feels are force from both the spring and the drag force from the water. After the spring fully extends, the torpedo only feels a force from the water. The dynamics of these two domains are analyzed separately.

Domain I ($0 < x < l$):

$$m\frac{d^2x}{dt^2} = k(l-x) - \frac{1}{2}\rho C_d A(\frac{dx}{dt})^2 \tag{16}$$

$$\frac{d^2x}{dt^2} + \frac{k}{m}x + \frac{1}{2}\rho\frac{C_dA}{m}(\frac{dx}{dt})^2 = \frac{k}{m}l \tag{17}$$

Domain II ($x > l$):

$$\frac{d^2x}{dt^2} + \frac{1}{2}\rho\frac{C_dA}{m}(\frac{dx}{dt})^2 = 0 \tag{18}$$

In this design, the compressed length of the spring is 1.25in and the torpedo starts from rest. This gives us the full set of differential equations and initial conditions that govern the dynamics of the torpedo. These equations are shown below and the MATLAB plots generated using ode45 are shown in Figure 1. The plots show that the torpedo will travel 1.5m (5ft) in about 3 seconds. This should provide enough range for the submarine.

$$\begin{cases} \frac{d^2x}{dt^2} + \frac{k}{m}x + \frac{1}{2}\rho\frac{C_dA}{m}(\frac{dx}{dt})^2 = \frac{k}{m}l & \text{if } 0 < \text{x} < \text{l}, \\ \frac{d^2x}{dt^2} + \frac{1}{2}\rho\frac{C_dA}{m}(\frac{dx}{dt})^2 = 0 & \text{if x} > \text{l}, \end{cases}$$

$$IC : x_0 = 1.25, v_0 = 0 \tag{19}$$

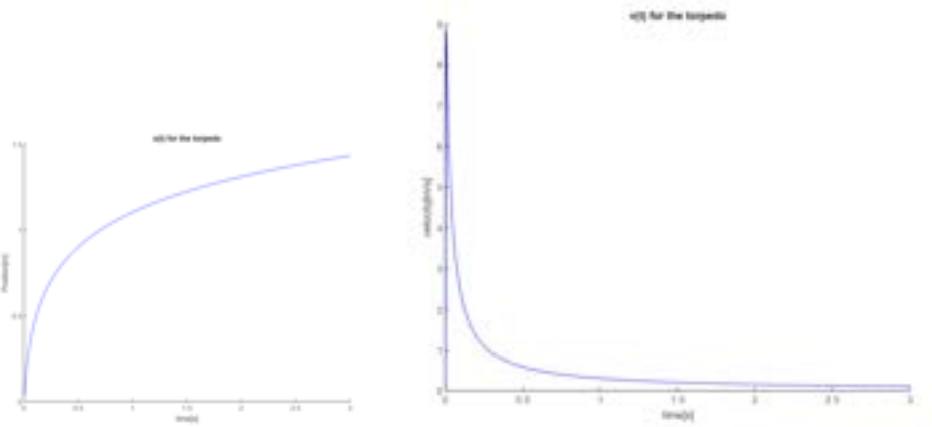

(a) Position of the torpedo (b) Velocity of the torpedo

Figure 15: MATLAB analysis of torpedo dynamics

C.2.3 Finite Element Analysis

I ran a SolidWorks simulation on the entire assembly to determine the stresses in the material caused by the torques from the torsion springs, and forces from the linear springs, torpedo weights, and dropper weights. This simulation was a static analysis of the system. I applied a 9 inlb torque from each torsion spring on its corresponding restraining finger. I also applied a 10 lb force on the torpedo restraining fingers to simulate the force from the compression springs. Finally, I applied a 0.5 lb downward force on each dropper restraining finger to simulate the weight of the dropper. I also fixed the frame bracket and the ends of both shafts to simulate the system's constraints. This simulation was performed to determine if the 3d printed parts could survive the loads from the springs. From the results below, we can see that the deformation is very low. I used the Additionally, the maximum stress occurs in the steel hex rod (as designed), so the safety factor is very high. This demonstrates that the system should handle the loads from the springs.

Table 6: Spring Load Analysis Data

Max Stress	26730 psi
Factor of Safety	22.2
Max Deformation	0.0245 in

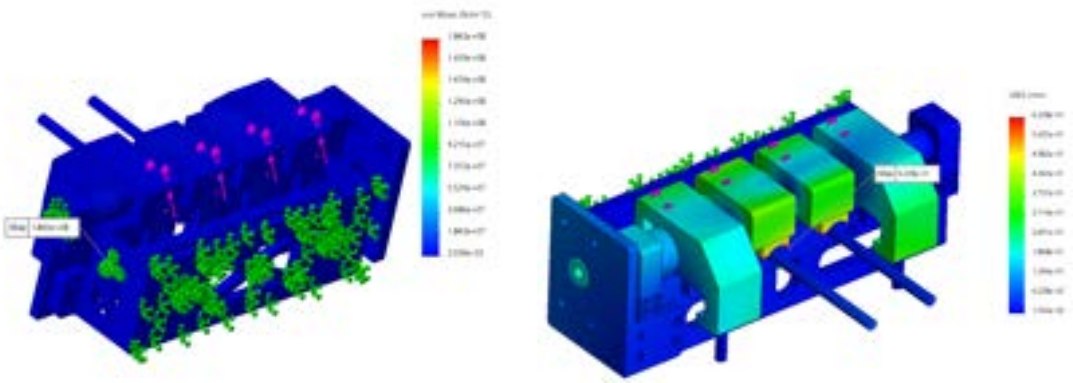

(a) Equivalent Von-Mises Stress (b) Total Deformation

Figure 16: Spring Load Analysis Simulation Results

D Polaris Manipulator

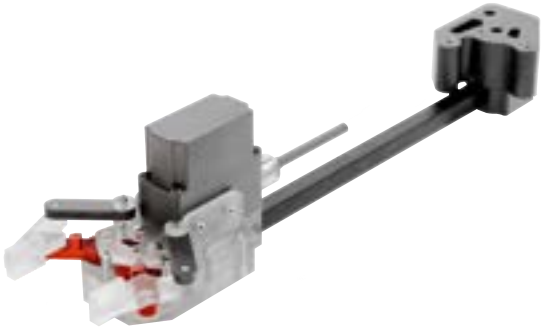

Figure 17: Polaris Manipulator

The Polaris manipulator allows the sub to pick up and move objects from the pool. This component is composed of a release mechanism, boom arm, and operable open-and-close claw driven via gears actuated by a SER-2020 servo.

D.1 Servo Gear- Axis Gear

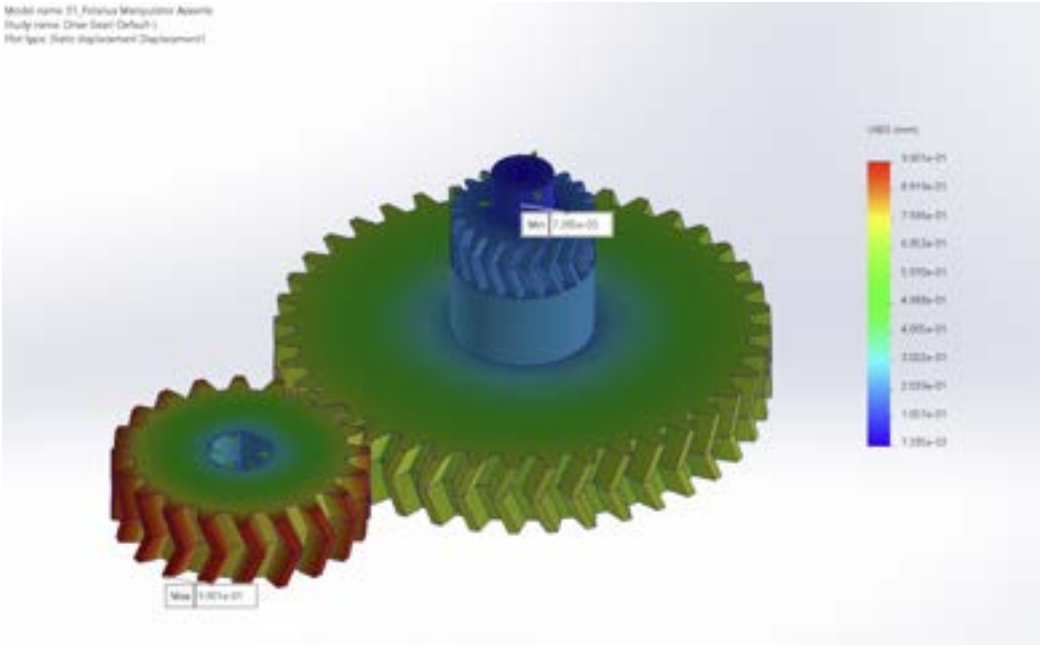

Figure 18: Sero Gear- Axis Gear Sim

Table 7: Servo-Axis Gear Analysis Data

Max Deformation	9.901e-01 mm
Applied Torque	3.3Nm

D.2 Axis Gear - Claw Gear

the deformation in this part seems excessive, but this is due to the four-bar linkage not in place. In other words, the 4.5mm deformation torque would be applied as clamping force, and the actual deformation on the assembly will not be 4mm. This simulation is to see if the top portion of the Axis gear and the Claw gear can withstand and transmit four times the torque from the servo.

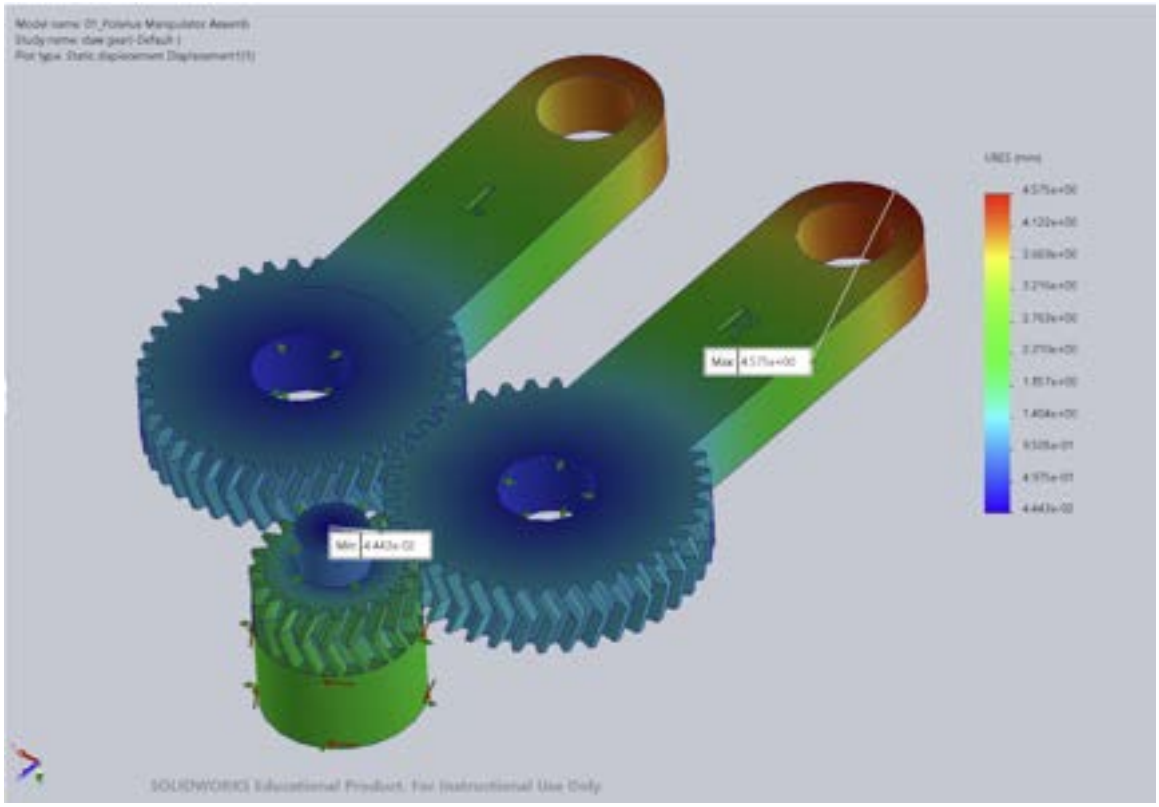

Figure 19: Axis Gear - Claw Gear Sim

Table 8: Axis Gear - Claw Gear Data

Max Deformation	4.575e-00 mm
Applied Torque	12.2Nm

D.3 Boom arm to frame plate

For some of the more important connections, topological studies are done before conducting weight reduction. This allow the removal of material to be safe, and the primary load-carrying portion will be kept.

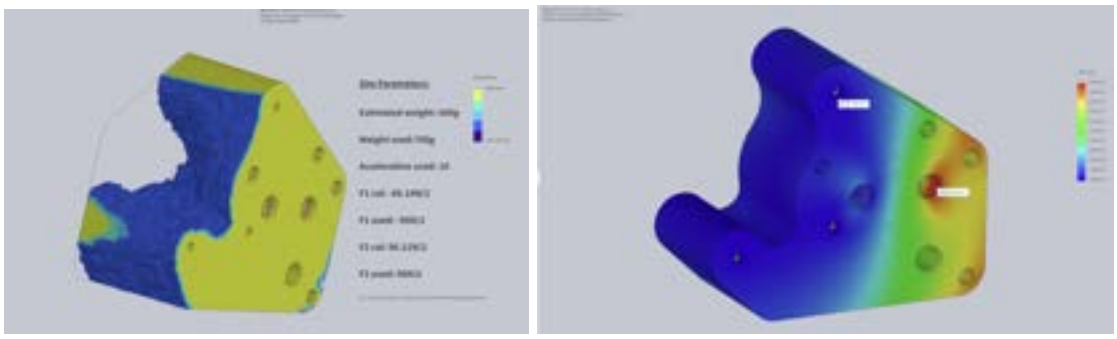

(a) to frame plate topological optimization (b) to frame plate sim

E Sirius Racks

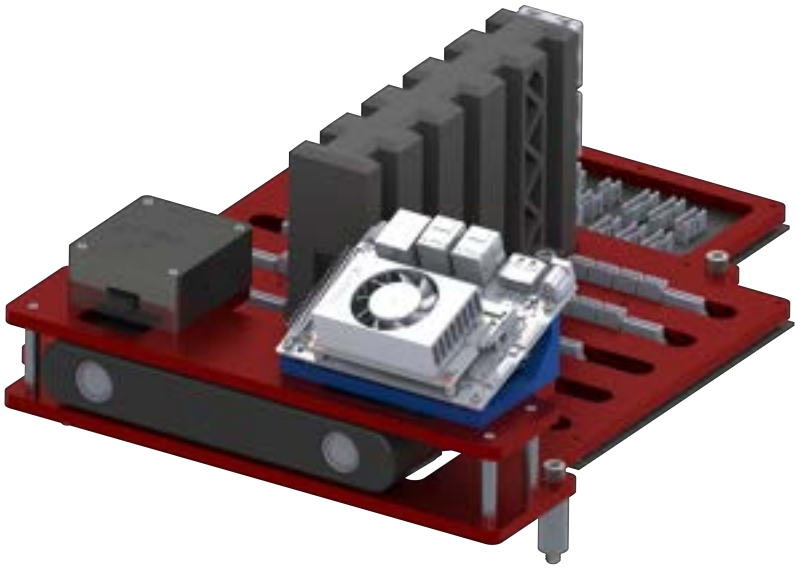

Figure 21: Sirius Racks

Sirius's racks feature a central tower for mounting custom circuit boards, 3D printed from Markforged Onyx for weight and manufacturing efficiency compared to aluminum. Onyx, a carbon fiber-reinforced nylon, offers superior rigidity and toughness compared to PLA or

ABS. Circuit boards are spaced 1.25” apart along the tower, secured with wedge locks in slots.

The tower mounts to an aluminum base plate routed to fit the hull floor, removable via four 1/4”-20 screws. A bridge on standoffs at the front of the plate supports Sirius’s forward camera, a Stereolabs Zed 2i, and above it, the vehicle’s Microstrain GX4 inertial measurement unit and Nvidia Jetson Orin Nano computer. The racks greatley differ from past designs due to the fact that they are made cor a lunchbox UHPV.

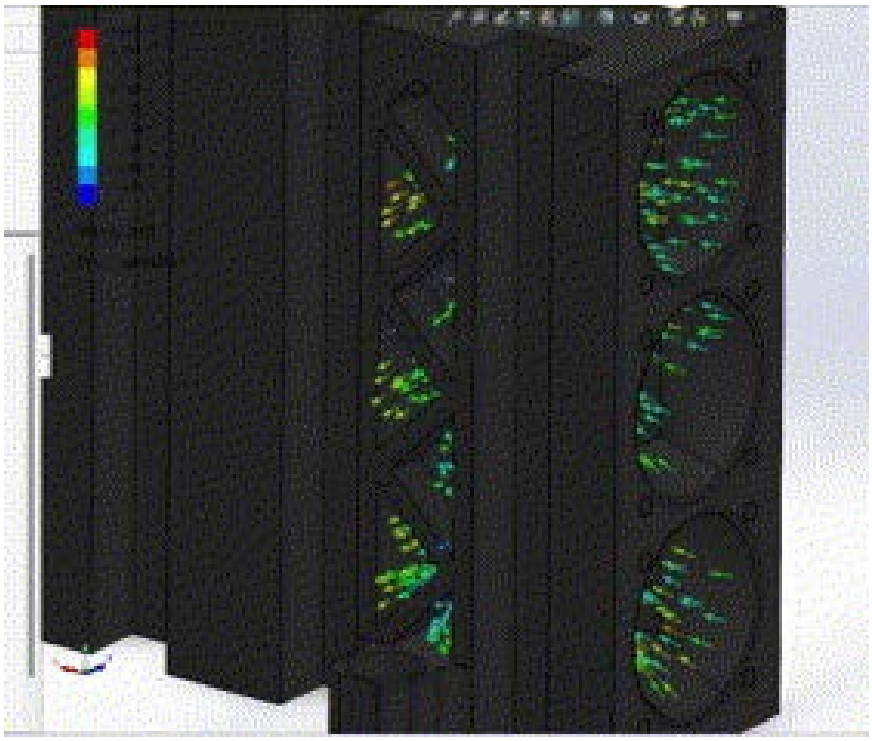

Figure 22: SolidWorks Flow simulation of air movement through the tower.

Table 9: Static simulation results.

Max Stress	715 psi
Location of Max Stress	Bridge Standoffs
Factor of Safety	56
Max Deformation	3.38E-4 in
Location of Max Deformation	Jetson Mount

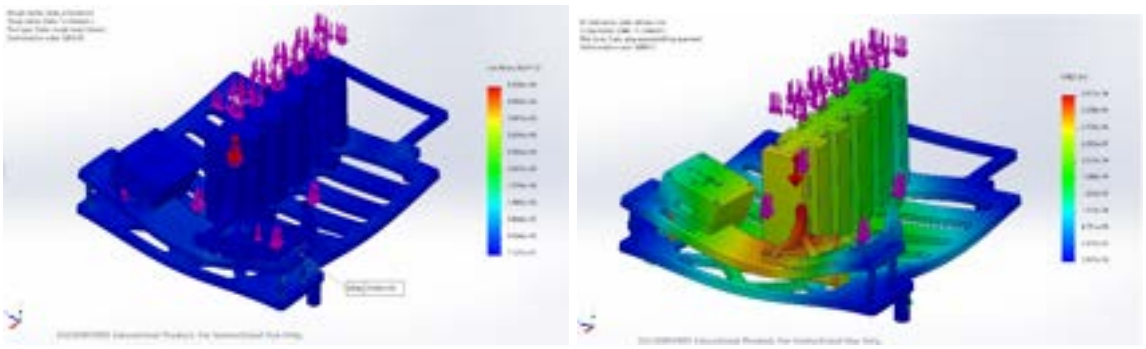

(a) Equivalent Von-Mises Stress (b) Total Deformation

Figure 23: Full assembly simulation results.

F Battery Pods

Figure 24: New Battery Pods

This year's battery pods make updates to an overall very strong last iteration. They also include a new system for integrating a battery management board with an LED screen to read out battery charge. The battery pods are one enclosure with a bore seal on one end. When opened, the lid and battery tray come out together, leaving nothing stuck in the

tube. This allows for easy access to everything inside the pods.

Figure 25: Tray with Battery Board and Battery

This year the battery board will be rectangular and will be mounted on the opposite side of the tray as the battery. This is a more efficient use of space as it fits more rectangles into the circular tube, but it poses some challenges. One challenge is that the battery board needs to be screwed into something. The tray is too thin, and there should not be screw heads sticking into the battery pods. My solution to this is four 3D-printed standoffs. They fit into 4 holes on the bottom of the tray and will face downwards. These standoffs hold heat-set inserts for 4-40 bolts that will hold the battery board in. They are designed to be epoxied to the tray. They taper to have as much material as possible holding the bolt and heat set insert, while having minimum contact with the underside of the battery board. The battery board and LED screen will be on the tray so that they are visible from the outside of the pod while it is standing on the endcap, which is how they are usually put down on tables.

Table 10: Simulation Analysis Data

Max Stress	28400 psi
Factor of Safety	14
Max Deformation	0.00244 in

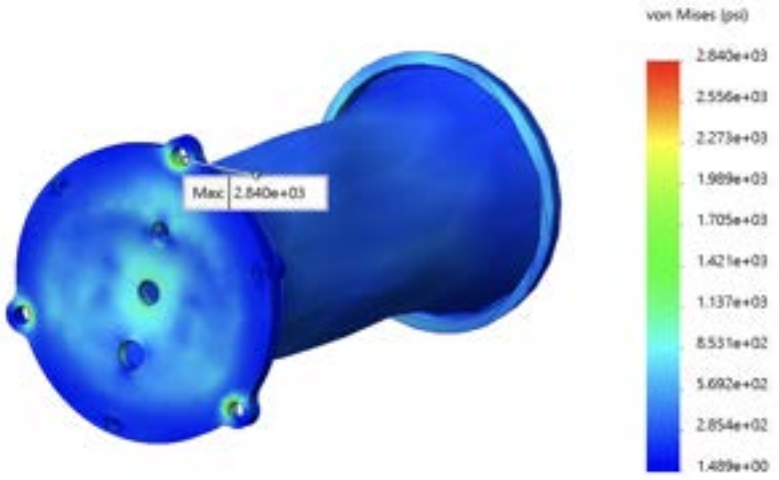

Figure 26: Stress Simulation

G Sirius UHPV (Upper Hull Pressure Vessel)

Figure 27: Sirius UHPV

This year's UHPV design for Sirius marks a significant departure from previous models. It will be a rectangular shape constructed from welded plates, accommodating more components than ever before. Despite being a minisub, Sirius will possess all the boards and capabilities of a full-size submarine. Integrating the ZED camera for forecam use, along with the IMU and killswitch, is a priority. The need for maneuverability dictates a square or rectangular enclosure for space efficiency, contrasting with traditional cylindrical designs

that waste volume.

Learning from past machining challenges past UHPV's and the necessity to increase size, manufacturing methods are being revised. Each plate of the UHPV will be machined in house, then outsourced to welders for final assembly. This approach reduces overall machining time and allows operations to be conducted in smaller, manageable stages. Key components include five side panels, a lid, and a separate collar to ensure bore seal integrity between the lid and UHPV hull.

G.1 UHPV Manufacturing

Each face of the UHPV was machined in house. There are the fore, back, port, starboard and bottom plates. The collar for the bore seal was machined separately to ensure the integrity of the bore seal. Each part was machined with the CNC Haas, though there had to be finishing manual operations. The UHPV was welded in Hillsboro, Oregon by HIS Innovations Group. This is the first time that CUAUV has designed a welded an enclosure and represents a major step in the CUAUV manufacturing capabilities.

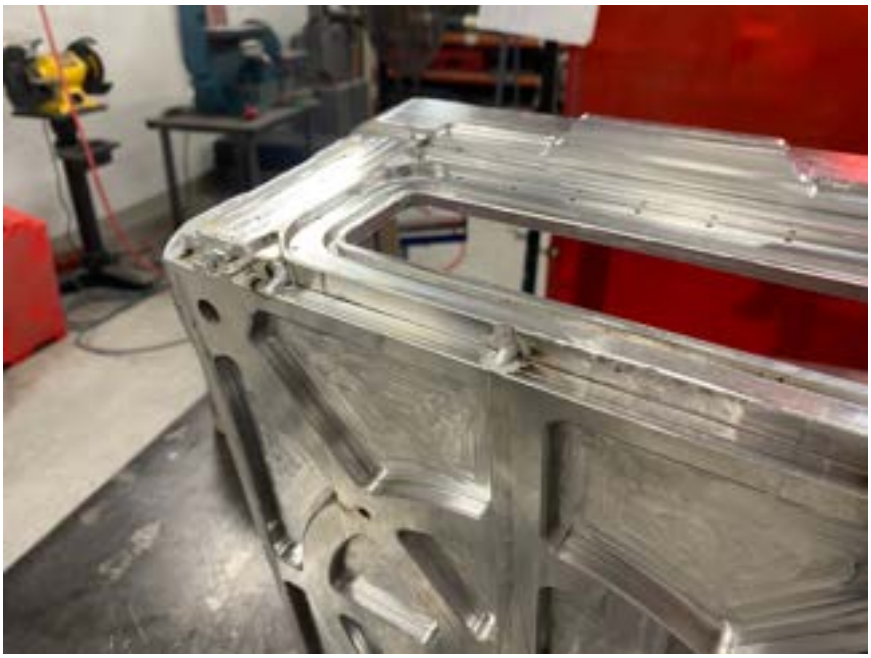

Figure 28: Tacks in Place

Figure 29: Weld Joint Finished

H Sirius Frame

The frame of the vehicle must take into account the new system advancements and requirements of all of the other projects. Sirius features the return of the lunchbox UHPV. The lunchbox is a square upper hull pressure vessel which has a sealing surface at the top. With this, in addition to the large view cone of the stereo ZED camera placed in the front of the sub, there are many differences between the thruster configuration and mounting holes of this Sirius compared to previous iterations. The eight thrusters sit in two different planes: four depth thrusters are attached to the side panels on the sub and the remaining thrusters are at the four corners (2 facing forwards and 2 facing backwards). Additionally, the Sirius frame features the introduction of a new actuation system using underwater servos to power the mechanisms. The GX4 IMU sensor is in the process of being integrated into the UHPV, and killswitch has also moved from its own enclosure to the back of the UHPV.

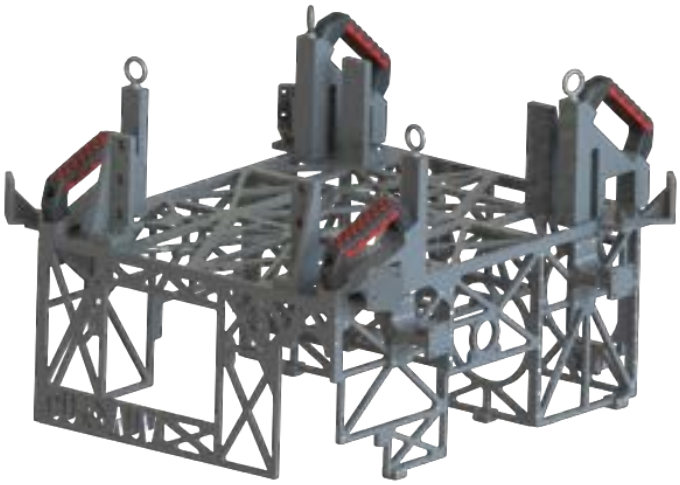

Figure 30: Sirius Frame

Many requirements that remain year-to-year are included in the design of Sirius's frame. The DVL must lie near the center of mass of the submarine at the bottom of the frame with ample room for its view-cone in order to take accurate velocity readings for software to use to control the sub; the down camera must be near the center as well in order to accommodate the software subteam's request to use the down facing camera as the center of rotation; hydrophones must be placed at the front corner of the sub, with its transducers pointing forward and down respectively and unobstructed by frame elements to allow for the transducers to be unobstructed while picking up signal; and the foreward camera must have a clear, unobstructed viewcone. See a list of enclosure and non-enclosures in Tables 1 and 2 below.

H.1 Table 1: List of Enclosures

Enclosure	Qty
UHPV	1
Hydrophones	1
Sensor Boom	1
Transmit	1
Downward Camera	1
Battery Pods	2

H.2 Table 2: List of Non-Enclosures

Enclosure	Qty
DVL	1
Handles	4
Torpedo-Dropper Enclosure	1
Thrusters	8
Eyebolts	4
Manipulator	1
Feet	6

I Sirius Downcam

Figure 1: Sirius Downcam

The downwards-facing camera (known as the "downcam") is a particularly useful sensor for the AUV which allows the vehicle to orient and align itself with particular game elements during missions. The enclosure which houses the downcam must contain enough space for the camera, lens, and wiring chosen for the specific design while also maintaining a watertight seal. The enclosure also needs to be mountable to either the UHPV or the frame, and be as small and lightweight as possible while also still being easy to maintenance in potentially time-sensitive situations. Typically, the downcam enclosure consists of five major components: a hull, flange, endcap, camera mounting bracket, and frame mounting bracket (if not directly attached to the UHPV).

I.1 Main Enclosure (Hull, Flange, Endcap) FEA

The main body of the enclosure, including the hull, flange, borosilicate glass, and endcap, was tested with an applied exterior pressure of 30 PSI, which is the approximate force that

the enclosure would experience at a depth of 50 feet. Even at a pressure which is well above the maximum that this enclosure is expected to ever experience, the factor of safety is above 40 and the enclosure shows little deformation (less than 1 thou). The maximum stress (994.1 PSI) is also comparable to previous camera enclosures (for reference, the yield strength of aluminium is approximately 35,000 PSI).

Table 1: Main Enclosure Analysis Data

Max Stress	994.1 PSI
Factor of Safety	40.12
Max Deformation	0.000467 in

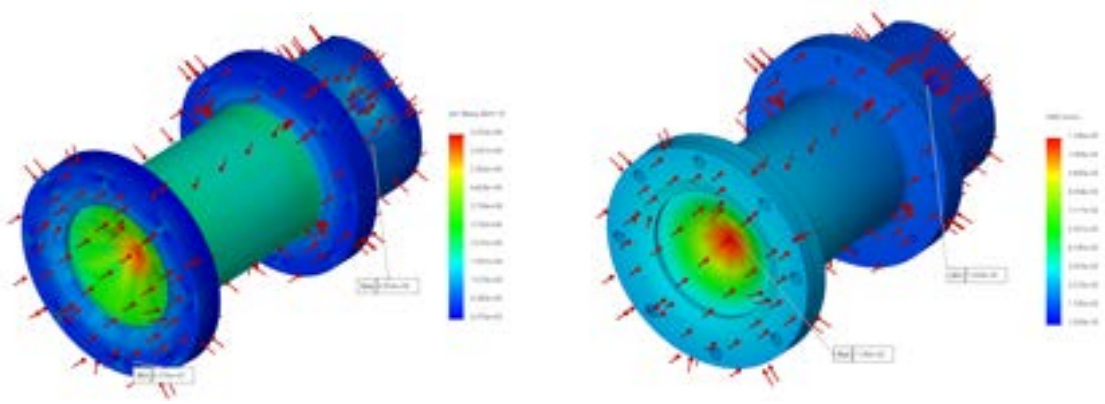

(a) Equivalent Von-Mises Stress (b) Total Deformation

Figure 2: Main Enclosure SolidWorks Simulation Results

I.2 Camera Mounting Bracket

The internal camera mounting bracket was also analyzed through static force and vibrational frequency SolidWorks simulations. In the static force study, a 10 N force (approximately 4 times the weight of the UI camera) was applied downwards along the face that the camera is mounted to. In this scenario (which could potentially occur during transport), the maximum stress (511.8 PSI) and deformation (0.003309 in) are still well within the acceptable limits for the 3D-printed PLA material (which has a yield strength of approx. 8,700 PSI and 6% elongation at break). In addition, this simulation assumed that bulkhead was not making contact with hull, which may further reduce the stress and deformation.

In the vibrational frequency simulation, a probing force of 5 N was applied to the thin exterior faces of the camera mounting bracket. Of the five generated modular shapes which SolidWorks produced, the two more relevant (lowest frequencies) are shown. The mode 1 frequency of 98 Hz could potentially be achieved during transit (such as on a bumpy road), but the addition of the bulkhead (which was also unbound in this simulation) should help to

mitigate these resonance issues. The twisting motion of mode 2 is not necessarily restricted by the bulkhead, but the resonant frequency of 272 Hz is unlikely to be achieved in either the transportation or operation of the AUV.

Table 2: Fore Endcap Analysis Data

Max Stress	511.8 PSI
Max Deformation	0.003309 in
Vibrational Frequency (Mode 1)	98.206 Hz
Vibrational Frequency (Mode 2)	272.15 Hz

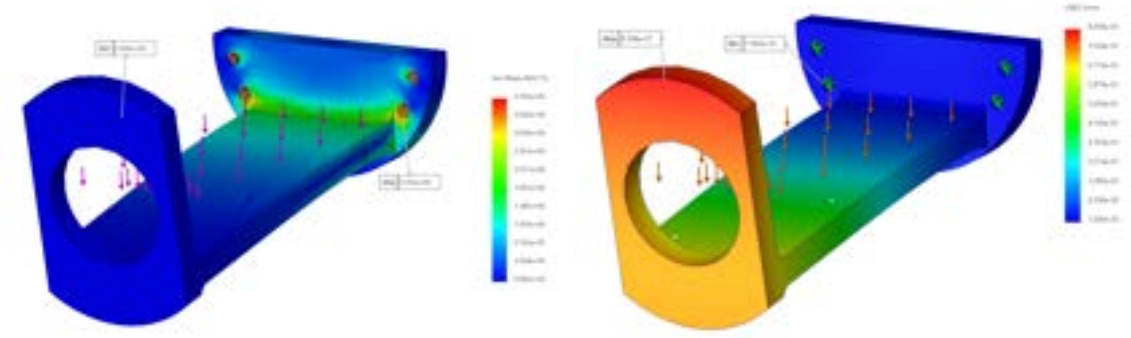

(a) Equivalent Von-Mises Stress (b) Total Deformation

Figure 3: Camera Mounting Bracket Static Force Simulation Results

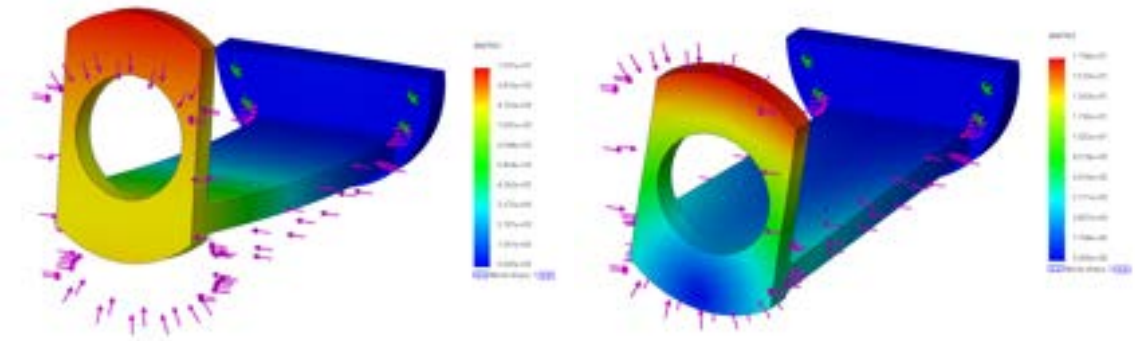

(a) Vibrational Frequency Mode 1 (b) Vibrational Frequency Mode 2

Figure 4: Camera Mounting Bracket Frequency Simulation Results